Sandia National Laboratories

Multi-task Machine Learning for Fusion Simulations

W. E. Lewis, A. Tran, K. Maupin, and P.F. Knapp

Introduction[1-4]

Magnetized Liner Inertial Fusion produces a hot (multi-keV), dense (~1 g/cc), and macroscopic (O(10mm) tall and O(0.1mm) diameter) cylindrical D_2 plasma. The fusion fuel at stagnation is well within the high energy density (HED) matter regime, with thermal pressures that can exceed 1Gbar.

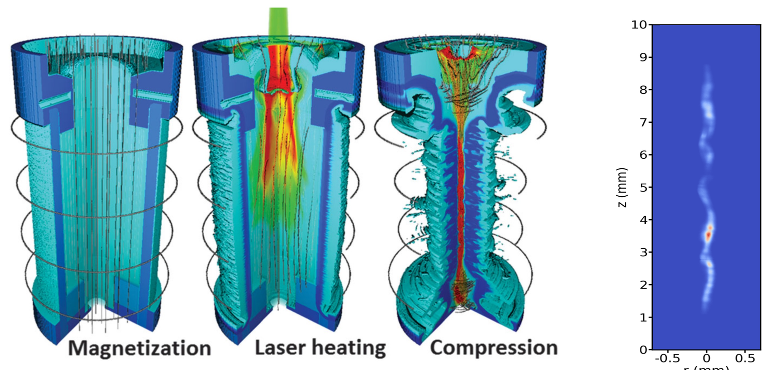

Extreme HED environments produced at Sandia's Z pulsed power facility place stringent constraints on diagnostic access and required robustness. Furthermore, experiments are costly, measurements are often highly spatially-spectrally- and/or temporally- integrated, and complex Multiphysics simulations are computationally expensive. These features represent significant challenges for experiment design and physics discovery.

Data-driven approaches are being developed to accelerate discovery and improve automation, uncertainty quantification, and reproducibility. Several published and ongoing projects[5-12] have demonstrated successful application to both experiment design and data analysis.

1D Magneto-Hydrodynamics Simulation Data[13]

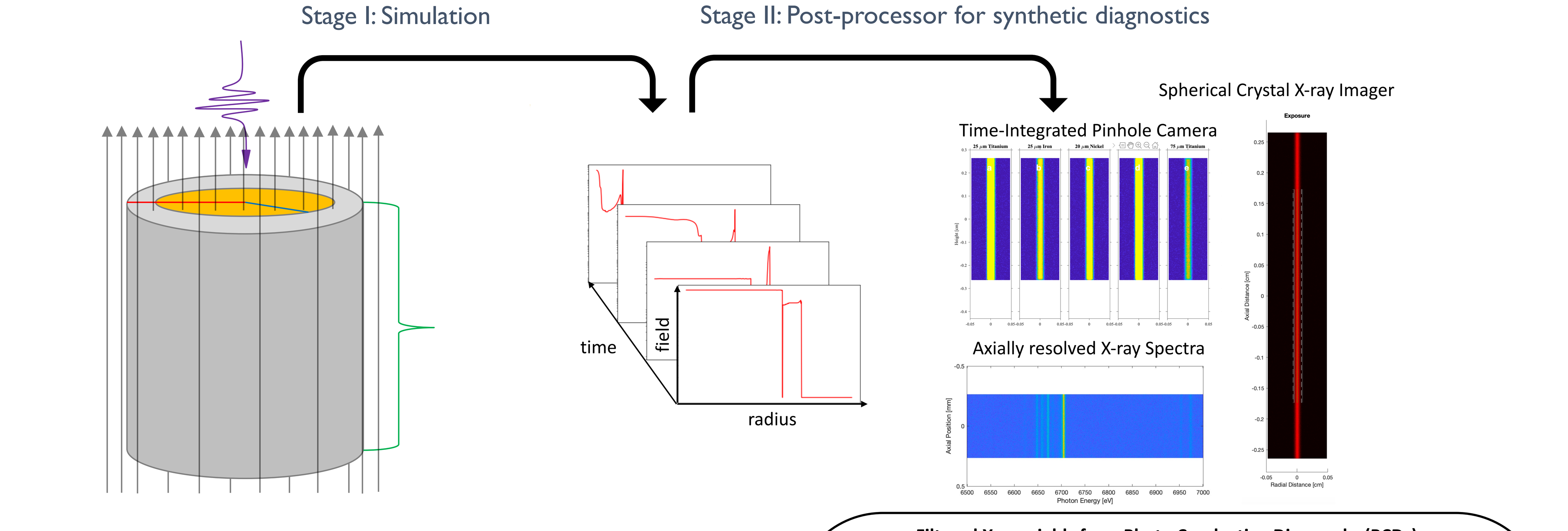

Inputs:
{R_o, R_i, E_{laser}, t_{laser}, Δt_{laser}, R_{laser}, B_z, ρ_{DD}, Z = 1cm}

Aspect ratio, $AR = \frac{R_o}{R_o - R_i}$ is used with R_i to compute R_o

Sampling Distribution:

- Laser energy deposited $\sim \mathcal{U}$ [500 J, 2kJ]
- Laser deposition start time $\sim \mathcal{U}$ [3020 ns, 3100 ns]
- Laser deposition duration $\sim \mathcal{U}$ [2ns, 6ns]
- Laser spot size $\sim \mathcal{U}$ [0.75mm, 1.5mm]
- Aspect ratio $\sim \mathcal{U}$ [4.5, 11]
- Inner liner radius $\sim \mathcal{U}$ [1.875 mm, 3.25 mm]
- Initial axial magnetic field strength $\sim \mathcal{U}$ [5T, 20T]
- Gas fill density $\sim \mathcal{U}$ [0.5mg/cc, 1.5mg/cc]

Filtered X-ray yields from Photo Conducting Diamond s (PCDs)

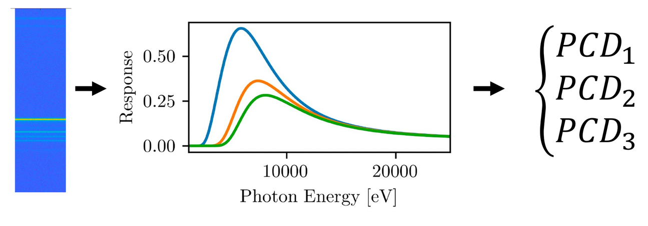

Filter x-rays

Instrument response space-time integration

DD Neutron yield

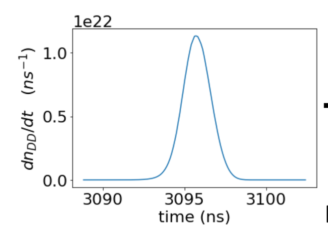

Instrument response space-time integration

Outputs are highly correlated and well suited for testing multi-task learning frameworks

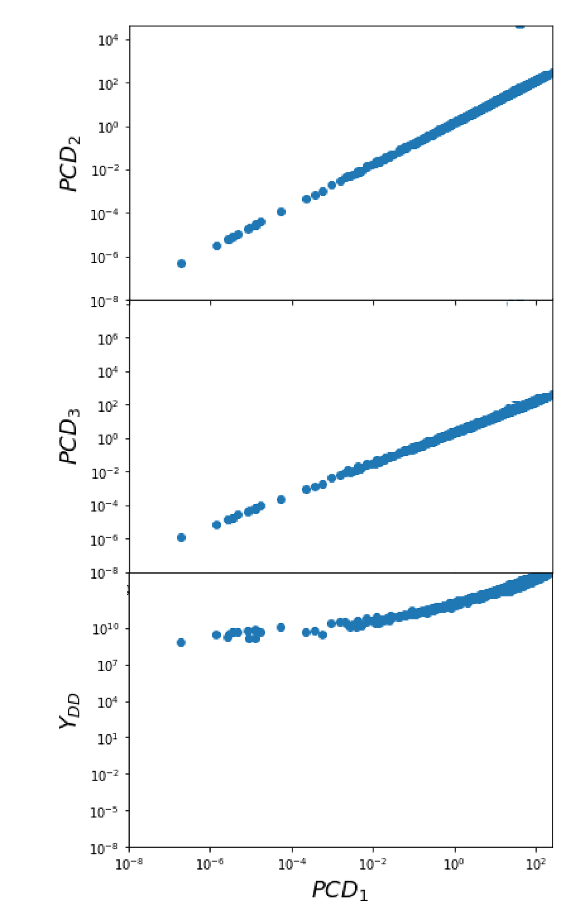

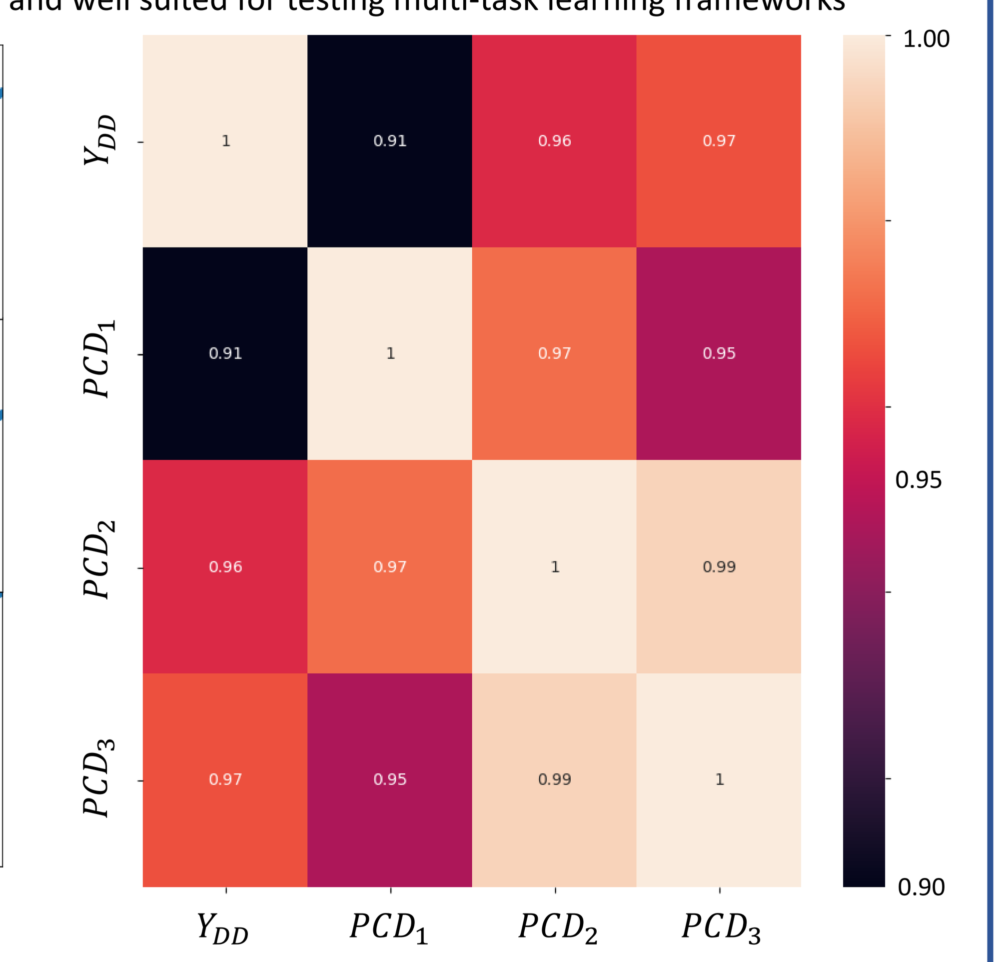

Additional details:

- Generated O(1000) samples for use in training and testing multi-output Gaussian processes
- Auto-adjusted laser deposition start time to avoid unphysical simulations
  - results in non-uniform final sample distribution
  - Removed O(10) outliers of unphysical origin
    - using the local outlier factor
  - Sampled AR uniformly
    - AR and R_i are GP inputs not R_o

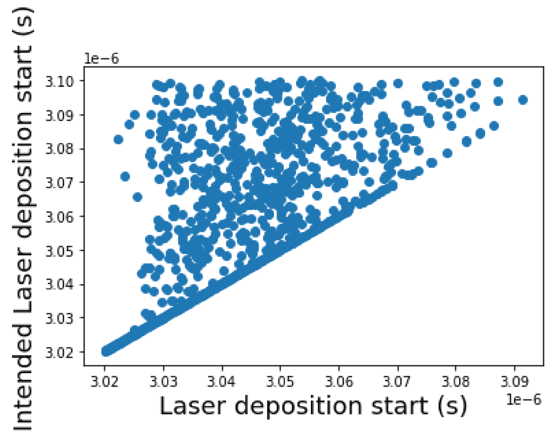

Single- and Multi-output Gaussian Processes[14,15]

Single-output

$$\mathbf{f} = [f(x_1), \ldots, f(x_N)]^T$$

$$P(\mathbf{f}) \sim \mathcal{N}(\mathbf{f}|\mathbf{m}, \mathbf{K}) \qquad P(\mathbf{y}|\mathbf{f}) \sim \mathcal{N}(\mathbf{y}|\mathbf{f}, \sigma\mathbf{I})$$

$$P(\mathbf{y}) = \int P(\mathbf{y}|\mathbf{f})P(\mathbf{f})d\mathbf{f} = \mathcal{N}(\mathbf{y}|\mathbf{m}, \mathbf{K} + \sigma\mathbf{I})$$

$$m(x_{n+1}) = \mu(x_{n+1}) + \mathbf{k}^T\mathbf{K}_n^{-1}\mathbf{y} \qquad \mathbf{k} = k(\mathbf{x}_n, x_{n+1}),$$

$$\sigma^2(x_{n+1}) = c - \mathbf{k}^T\mathbf{K}_n^{-1}\mathbf{k} \qquad \mathbf{K}_{Ni,j} = k(x_i, x_j) + \sigma\delta_{i,j}(i, j = 1 \ldots n)$$

$$c = k(x_{n+1}, x_{n+1}) + \sigma$$

$$\log p(\mathbf{y}|\mathbf{X}, \theta) = -\frac{N}{2}\log 2\pi - \frac{1}{2}\log|\mathbf{K}(\mathbf{X},\mathbf{X}) + \sigma^2\mathbf{I}| - \frac{1}{2}(\mathbf{y}-\mathbf{m})^T[\mathbf{K}(\mathbf{X},\mathbf{X}) + \sigma^2\mathbf{I}]^{-1}(\mathbf{y}-\mathbf{m})$$

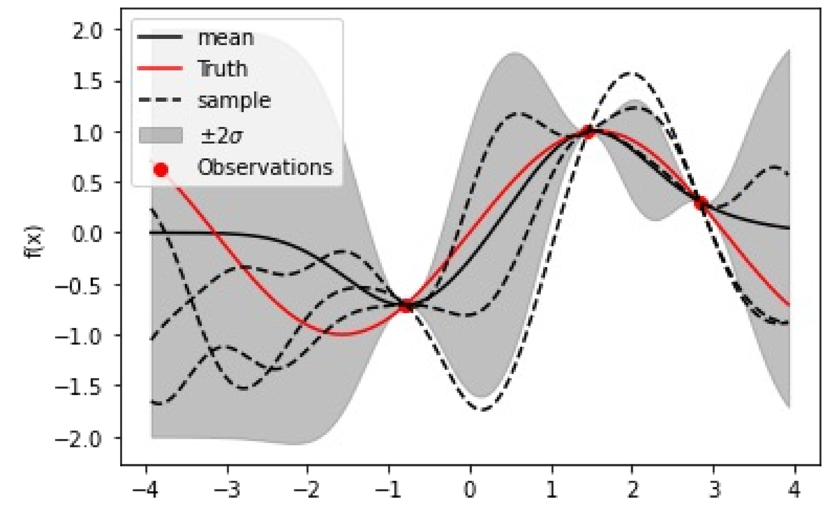

Note that posterior prediction requires inversion of NxN kernel matrix where N is the number of observed data points

Multi-output

$$\mathbf{f} = [f_1, \ldots, f_T]^T \qquad \mathbf{f}(\mathbf{X}) \sim \mathcal{N}(\mathbf{m}(\mathbf{X}), \mathbf{K}(\mathbf{X},\mathbf{X}))$$

$$p(\mathbf{y}|\mathbf{f}, \mathbf{x}, \Sigma) = \mathcal{N}(\mathbf{f}(\mathbf{x}), \Sigma) \qquad p(\mathbf{f}(x_*)|\mathbf{y}) = \mathcal{N}(\mathbf{f}_*(x_*), \mathbf{K}_*(x_*, x_*))$$

$$\mathbf{f}_*(x_*) = \mathbf{K}_{x_*}^\top[\mathbf{K}(\mathbf{X},\mathbf{X}) + \boldsymbol{\Sigma}]^{-1}(\mathbf{y}-\mathbf{m}),$$

$$\mathbf{K}_*(x_*, x_*) = \mathbf{K}(x_*, x_*) - \mathbf{K}_{x_*}[\mathbf{K}(\mathbf{X},\mathbf{X}) + \boldsymbol{\Sigma}]^{-1}\mathbf{K}_{x_*}^\top$$

$$\log p(\mathbf{y}|\mathbf{X}, \theta) = -\frac{ND}{2}\log 2\pi - \frac{1}{2}\log|\mathbf{K}(\mathbf{X},\mathbf{X}) + \boldsymbol{\Sigma}| - \frac{1}{2}(\mathbf{y}-\mathbf{m})^\top[\mathbf{K}(\mathbf{X},\mathbf{X}) + \boldsymbol{\Sigma}]^{-1}(\mathbf{y}-\mathbf{m})$$

Note that posterior prediction requires inversion of NTxNT kernel matrix where N is the number of observed data points and T is number of outputs.

$$u_q^i \sim \mathcal{GP}(0, k_q(\mathbf{x}, \mathbf{x}'))$$

	LMC	ICM	SLFM
$f_t(x) =$	$\sum_{q=1}^{Q}\sum_{i=1}^{R_q} a_{t,q}^i u_q^i(\mathbf{x})$	$\sum_{i=1}^{R} a_t^i u^i(\mathbf{x})$	$\sum_{q=1}^{Q} a_{t,q} u_q(\mathbf{x})$
$cov[\mathbf{f}(\mathbf{x}), \mathbf{f}(\mathbf{x}')] =$	$\sum_{q=1}^{Q} \mathbf{B}_q k_q(\mathbf{x}, \mathbf{x}')$	$\mathbf{B}k(\mathbf{x}, \mathbf{x}')$	$\sum_{q=1}^{Q} \mathbf{B}_q k_q(\mathbf{x}, \mathbf{x}')$
$\mathbf{A}_{(q)} =$	$[\mathbf{a}_q^1\, \mathbf{a}_q^2 \ldots \mathbf{a}_q^{R_q}]$	$[\mathbf{a}^1\, \mathbf{a}^2 \ldots \mathbf{a}^R]$	$\mathbf{a}_q$

$$\mathbf{B}_q = \mathbf{A}_q\mathbf{A}_q^T$$

Results

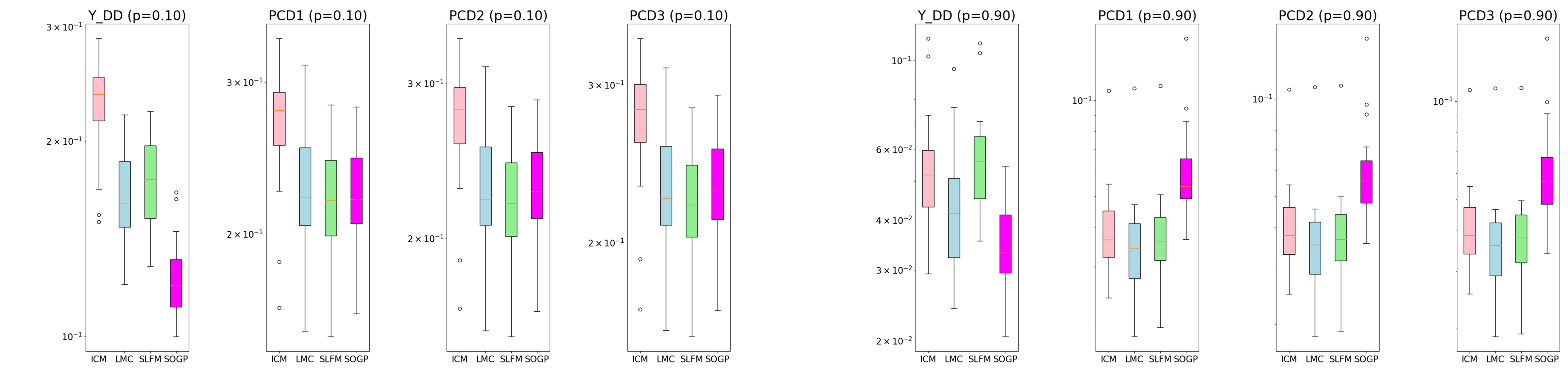

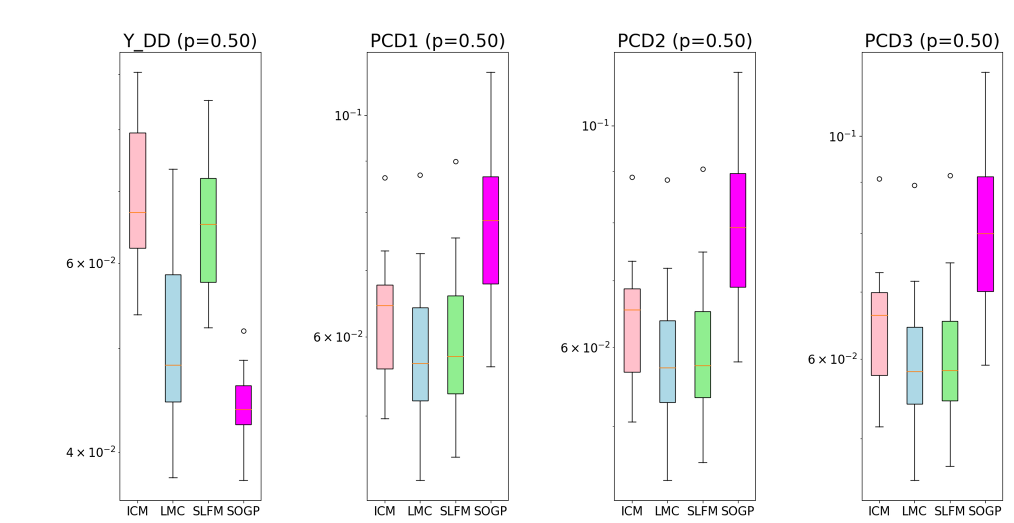

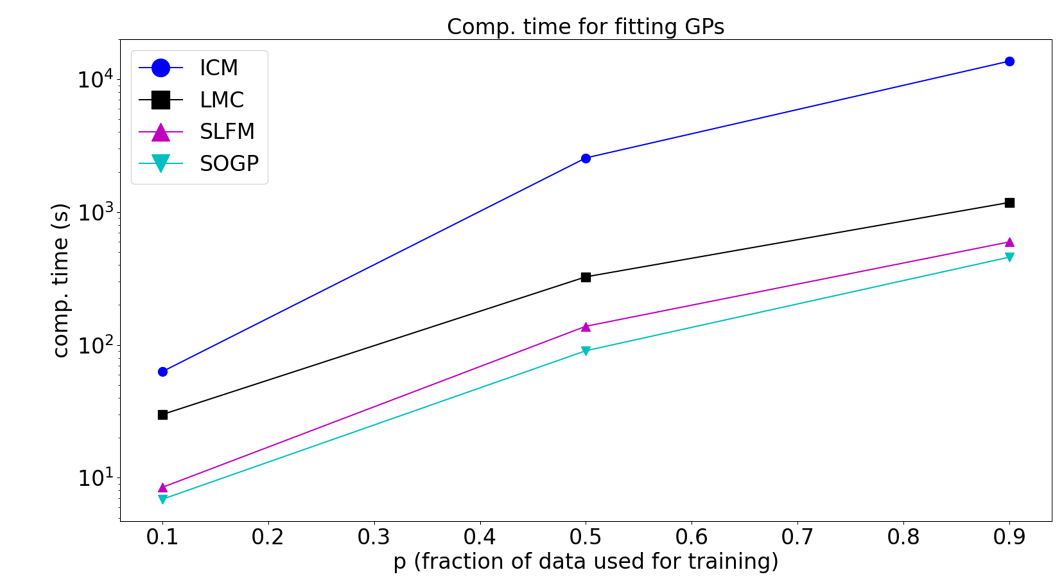

Conclusions

- MOGPs generally outperform the SOGP on PCD values, while performing comparably or worse on Y_{DD}
- Computational cost of MOGPs is competitive with SOGPs, with ICM being the most expensive

[1] S.A. Slutz *et al.*, Phys. Plasmas **17**, 056303 (2010).
[2] M.R. Gomez *et al.*, Phys Rev. Lett. **113**, 155003 (2014).
[3] M.R. Gomez *et al.*, Phys. Rev. Lett. **125**, 155002 (2020).
[4] D. Yager-Elorriaga *et al.*, Nucl. Fusion **62**, 042015 (2021).
[5] W.E Lewis *et al.*, Phys. Plasmas **28**, 092701 (2021).
[6] P.F. Knapp *et al.*, Phys. Plasmas **29**, 052711 (2022).
[7] P.F. Knapp *et al.*, J. Plasma Phys. (under review).
[8] J.R. Fein *et al.*, In Preparation.
[9] W.E. Lewis *et al.*, J. Plasma Phys. (under review).
[10] W.E. Lewis *et al.*, In Preparation.
[11] M.E. Glinsky *et al.*, Phys. Plasmas **27**, 112703 (2020).
[12] D.J. Ampleford *et al.*, In Preparation.
[13] C. Jennings *et al.*, Phys. Plasmas **17**, 092703 (2010).
[14] C.E. Rasmussen and C.K.I. Williams, Gaussian Processes for Machine Learning, MIT Press (2005).
[15] M.A. Alvarez and N.D. Lawrence, J. Machine Learning Research **12**, 1459 (2011).

Sandia National Laboratories is a multimission laboratory managed and operated by National Technology &Engineering Solutions of Sandia, LLC, a wholly owned subsidiary of Honeywell International Inc., for the U.S. Department of Energy's National Nuclear Security Administration under contract DE-NA0003525.

SAND2022-#### C